Effects of Fluorination on Fused Ring Electron Acceptor for Active Layer Morphology, Exciton Dissociation, and Charge Recombination in Organic Solar Cells

Hou, Licheng; Lv, Jie; Wobben, Friso; Le Corre, Vincent M.; Tang, Hua; Singh, Ranbir; Kim, Min; Wang, Fufang; Sun, Haitao; Chen, Wenjing

Published in:
ACS Applied Materials & Interfaces

DOI:
10.1021/acsami.0c16411

Publication date:
2020

ACS APPLIED MATERIALS & INTERFACES

www.acsami.org

Research Article

Effects of Fluorination on Fused Ring Electron Acceptor for Active Layer Morphology, Exciton Dissociation, and Charge Recombination in Organic Solar Cells

Licheng Hou, Jie Lv, Friso Wobben, Vincent M. Le Corre, Hua Tang, Ranbir Singh,* Min Kim, Fufang Wang, Haitao Sun, Wenjing Chen, Zhengguo Xiao, Manish Kumar, Tongle Xu, Weimin Zhang, Iain McCulloch, Tainan Duan, Huling Xie, L. Jan Anton Koster, Shirong Lu,* and Zhipeng Kan*

Cite This: *ACS Appl. Mater. Interfaces* 2020, 12, 56231−56239

Read Online

ACCESS | Metrics & More | Article Recommendations | Supporting Information

ABSTRACT: Fluorination is one of the effective approaches to alter the organic semiconductor properties that impact the performance of the organic solar cells (OSCs). Positive effects of fluorination are also revealed in the application of fused ring electron acceptors (FREAs). However, in comparison with the efforts allocated to the material designs and power conversion efficiency enhancement, understanding on the excitons and charge carriers' behaviors in high-performing OSCs containing FREAs is limited. Herein, the impact of fluorine substituents on the active layer morphology, and therefore exciton dissociation, charge separation, and charge carriers' recombination processes are examined by fabricating OSCs with PTO2 as the donor and two FREAs, O-IDTT-IC and its fluorinated analogue O-IDTT-4FIC, as the acceptors. With the presence of O-IDTT-4FIC in the devices, it is found that the excitons dissociate more efficiently, and the activation energy required to split the excitons to free charge carriers is much lower; the charge carriers live longer and suffer less extent of trap-assisted recombination; the trap density is 1 order of magnitude lower than that of the nonfluorinated counterpart. Overall, these findings provide information about the complex impacts of FREA fluorination on efficiently performed OSCs.

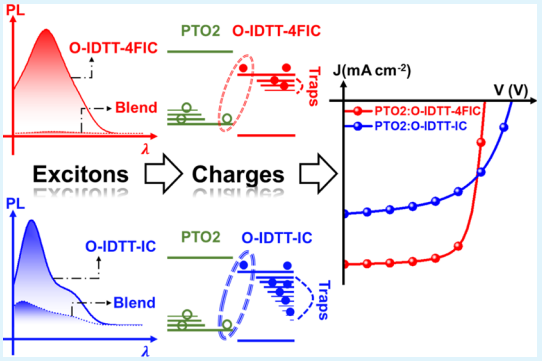

KEYWORDS: *fluorination, exciton dissociations, activation energy, trap assisted recombination, crystallinity*

1. INTRODUCTION

The power conversion efficiency (PCE) of organic solar cells (OSCs) higher than 13% were reported with nonfullerene acceptors and novel donors' designs.[1−5] Especially, with the emergence of Y6,[6] a fused ring electron acceptor (FREA), PCE up to 18.2% was obtained in single-junction OSCs.[7,8] Considering the properties of OSCs such as solution-processable fabrications, flexible devices, tunable light harvesting ranges, and scalability, OSCs are a competitive candidate for complementary applications on the scenarios that the inorganic counterparts cannot be applied.[9−11] In comparison with other kinds of thin-film solar cells, the major limiting factor of OSCs is the PCE, and therefore, it is of great importance to improve the OSC performance.

Besides device engineering and light management in improving the OSC efficiency, great efforts are contributed to the novel donor/acceptor material design to tune the properties of the organic semiconductors for desirable energy levels, absorption profiles, and aggregation features.[12] Because of the strong electron-withdrawing natures and planar conformation of the molecules, fluorine substitution is one of the effective methods to manipulate these properties of organic semiconductors.[13] When fullerene derivatives were used as the electron acceptor, the fluorination attempts were mainly on the donor materials. With fluorine (F) atom substituted in the backbone of the donors, the highest occupied molecular orbital (HOMO) energy levels is lower than that of the donors without an F substituent, which may result in improved open-circuit voltage (V_{OC}) of the fabricated OSCs.[14−17] In addition, the molecular packing properties usually changed to have strong tendency to aggregate, form more face-on oriented crystallites, and improve molecular ordering, leading to improved charge carrier mobility. With these benefits, the OSCs composed of the fluorinated counterparts often have larger V_{OC}, short circuit current density (J_{SC}), and fill factor (FF), resulting from the less extent of bimolecular recombination and reduced geminate recombination.[14,18]

Received: September 11, 2020
Accepted: November 20, 2020
Published: December 3, 2020

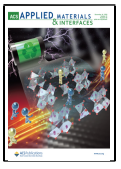

https://dx.doi.org/10.1021/acsami.0c16411
ACS Appl. Mater. Interfaces 2020, 12, 56231−56239

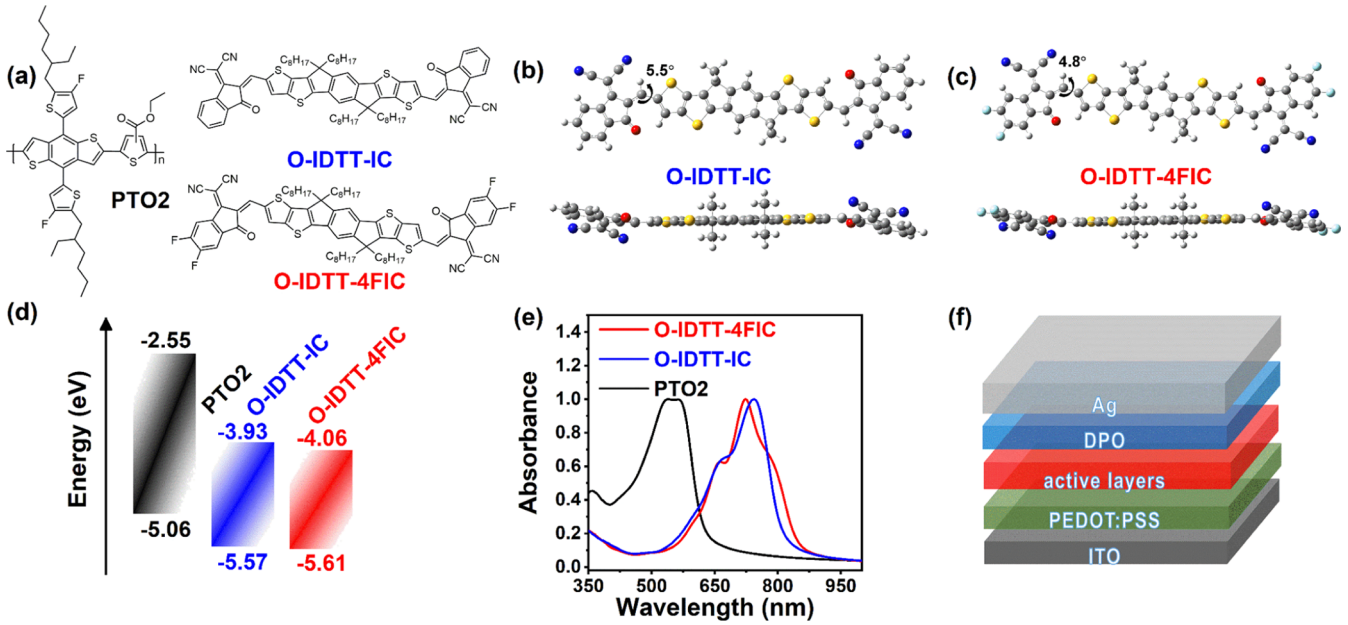

Figure 1. (a) Chemical structures of PTO2, O-IDTT-IC, and O-IDTT-4F IC. (b) Ground-state geometries of O-IDTT-IC. (c) Ground-state geometries of O-IDTT-4FIC. (d) Energy levels of the donor and the acceptors determined by CV measurement. (e) Normalized absorbance spectra of the pristine films of the donor and acceptors. (f) Device architecture.

The positive effects by the introduction of F were also revealed in OSCs with FREAs.[19] In this kind of OSCs, the element substitution can be both applied to the donors and the acceptors. Particularly, when the fluorination approach was applied to the FREAs, it was found that the F-substituent can down shift the lowest unoccupied molecular orbital (LUMO) energy levels, red-shift the absorption in solid films, and enhance intermolecular interactions, including the improved molecular packing properties.[18,20−22] It is worth noting that the V_{OC} was normally lower than that of the nonfluorinated counterparts because of the lower-lying LUMO.[21,23] In the operation of OSCs with fluorinated FREAs, it was reported that fluorination helped to suppress the energetic disorder and prolong the carrier lifetime and thus aid charge extraction.[24,25] With increased number of the F atoms in the FREAs' backbones, the difference of the electrostatic potential between the donor and acceptor can increase, causing enhanced donor/acceptor interactions, and PCE as high as 16.7% was achieved with such designs. Taking into account above mentioned advantages, fluorination has great potential for constructing high-performance OSCs, and therefore, the deeper understanding of the structure−property relationships induced by fluorination is critical. It is also noted that fluorination has been widely applied in nearly all the high-performed FREAs beyond 13%.[26−29] However, in comparison with the efforts allocated to the material designs and emphasis of PCE enhancement, those assigned to understand the structure−properties in device operations were limited. Notably, excitons and charges' behaviors such as the activation energy for splitting the excitons, nongeminate recombination processes, charge extraction, and charge carriers' lifetime, which directly determine the device performance and link the microstructures with the device properties of high-performing OSCs with FREAs, were less reported.

In this contribution, we examined the impact of F on the microstructure−electrical property relationships by fabricating OSCs with PTO2 as the electron donor and two FREAs O-IDTT-IC and its fluorinated analogue O-IDTT-4FIC as the electron acceptors. It was found that the pristine film of O-IDTT-IC shows preferred face-on orientation crystallites and the pristine film of O-IDTT-4FIC presents bimodal oriented crystallinity. When these morphological effects were translated into the active layers, the FF significantly changed from 56 to 74%. On the other hand, the devices with O-IDTT-4FIC as the acceptor showed higher J_{SC} and lower V_{OC} than those of the nonfluorinated counterpart, which were in line with the red shift absorption and the lower lying LUMO level introduced by the fluorination. As a result, the devices with PTO2:O-IDTT-4FIC as the active layer achieved a PCE of 14.5%, outperforming the device with PTO2:O-IDTT-IC as the active layer (9.1%). In addition, we found that the exciton dissociation efficiency in the active layer with PTO2:O-IDTT-4FIC were much higher, and less activation energy was required to generate free charge carriers (36.7 meV vs 53.5 meV); trap-assisted recombination are the major loss channel for both device systems, whereas bimolecular recombination is negligible; the charge extraction times of both devices were comparable (0.98 μs vs 0.81 μs), while the devices with PTO2:O-IDTT-4FIC showed a much longer charge carrier lifetime (3.04 μs vs 1.22 μs), indicating significantly reduced trap-assisted recombination; the one-dimensional (1D) simulation further confirmed that the trap density in the active layer of PTO2:O-IDTT-4FIC was one order lower than that of the active layer with PTO2:O-IDTT-IC. Our findings provide information into the complex effects of FREA fluorination in high-performance OSCs.

2. RESULTS AND DISCUSSION

The molecular structures of PTO2, O-IDTT-IC, and O-IDTT-4FIC are plotted in Figure 1a. The top and side views of the ground-state geometries of O-IDTT-IC and O-IDTT-4FIC are pictured in Figure 1b,c, showing more planner conformation with F substituents.[30−32] Figure 1d presents the normalized absorbance spectra of PTO2, O-IDTT-IC, and O-IDTT-4FIC

https://dx.doi.org/10.1021/acsami.0c16411
ACS Appl. Mater. Interfaces 2020, 12, 56231−56239

in pristine films. The absorption of PTO2 in thin film covers from *ca.* 350 to 650 nm. In comparison with the solid film of O-IDTT-IC, the film of O-IDTT-4FIC shows notably higher absorption in the long wavelength range with the absorption onsets approximately at 870 nm. The absorption ranges of the donor and acceptors complement each other well. The energy levels determined by cyclic voltammetry (CV) measurement are summarized in Figure 1e. The HOMO and LUMO levels of O-IDTT-IC, and O-IDTT-4FIC are −5.57/3.93 and −5.61/-4.06 eV, corresponding to the band gap of 1.55 and 1.64 eV, respectively. The red shift absorption and lower-lying LUMO level are well in line with other reports.

As shown in Figure 1f, to demonstrate the photovoltaic performance of O-IDTT-4FIC and O-IDTT-IC in OSCs, the conventional devices with the architecture of glass/ITO/PEDOT:PSS/active layer/phenyl(2-naphthyl)-diphenylphosphine oxide (DPO)/Ag were fabricated. The optimization processes and details are detailed in Tables S1−S6. Figure 2a shows the current density−voltage (*J*−*V*) curves

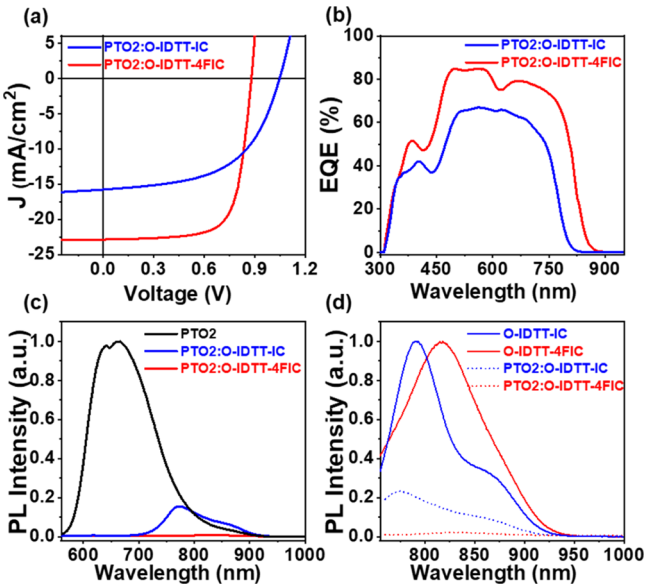

Figure 2. (a) *J*−*V* curves of devices with PTO2:O-IDTT-IC and PTO2:O-IDTT-4FIC as the active layer. (b) EQE spectra of the devices with PTO2:O-IDTT-IC and PTO2:O-IDTT-4FIC. (c) Steady-state PL spectra when the donor was excited. (d) Steady-state PL spectra when the acceptors were excited.

of the optimal devices, and the photovoltaic parameters of the optimized OSCs under simulated AM1.5G irradiation (100 mW cm^{-2}) are summarized in Table 1. In detail, the PCE of devices with PTO2:O-IDTT-IC as the active layer is 9.11% with a V_{OC} of 1.03 V, a J_{SC} of 15.78 mA cm^{-2}, and an FF of 56.10%. When the F substituent was introduced, the performance of the device dramatically improved.

The devices with PTO2:O-IDTT-4FIC as the active layer yielded a V_{OC} of 0.86 V, a J_{SC} of 22.87 mA cm^{-2}, and an FF of 74.05%, leading to a much higher PCE of 14.51%. The lower V_{OC} from the devices with fluorinated acceptor agrees well with the lower-lying LUMO, and the improved J_{SC} is attributed to the red shift absorption as shown in the external quantum efficiency (EQE) spectra. Besides the changes in V_{OC} and J_{SC}, the FF had an improvement of *ca.* 20%, and we assign this to the morphological changes which will be discussed in later sections.

Figure 2b exhibits the EQE responses of the champion devices. The spectrum of the device with O-IDTT-4FIC is wider than that of the device with O-IDTT-IC, which confirms the red-shifted absorption characteristics of O-IDTT-4FIC. In the range of 400−850 nm, the device with O-IDTT-4FIC exhibits higher response than that of the device with O-IDTT-IC, proving the higher J_{SC} measured by the solar simulator from the device with O-IDTT-4FIC. In addition, the maximum EQE response of the device with O-IDTT-4FIC is *ca.* 85%, which is significantly higher than the EQE of the control device (*ca.* 66%). On the other hand, internal quantum efficiency (IQE) characteristics, defined as the ratio of the number of charge carriers extracted from the device to the number of photons absorbed in the active layer, can provide insightful information about the electrical properties of solar cells that EQE measurements alone cannot.[33] IQE is usually determined by combined simulation and experimental way, or it can be also estimated as the ratio of experimental J_{SC} to the maximum theoretical J_{SC} obtained from transfer matrix model simulation (detailed in Section S5).[34] The IQE values of *ca.* 92% and *ca.* 71% were calculated for devices with O-IDTT-4FIC and O-IDTT-IC, respectively. Because IQE measurements normalize the current generation efficiency by the light absorption efficiency, the nearly 20% differences in IQE is related with the exciton dissociation and charge recombination.

To verify the origin of the distinct device performance, the excitons and the charge carriers' behaviors that govern the device performances were examined. The excitons to the charge carrier process was monitored by performing the photoluminescence (PL) measurements on the pristine and blend films, and the normalized PL spectra are depicted in Figure 2c,d. When the donor material PTO2 was photoexcited (Figure 2c), energy transfer from the PTO2 to the acceptors happened and followed by hole transfer back; while the acceptors were photoexcited (Figure 2d), hole transfer from the acceptors to the donor happened. Thus, the PL quenching (PLQ) efficiency observed was determined by the competition of hole transfer and exciton recombination no matter which component was photoexcited. Because of the large HOMO−HOMO offset, it was observed that the PLQ efficiency of the active layer with PTO2:O-IDTT-4FIC is much higher than that of the active layer with PTO2:O-IDTT-IC.[35,36] These results suggest that the excitons generated upon photons absorbed can dissociate efficiently to free charge carriers in the film of PTO2:O-IDTT-4FIC. On the contrary, the excitons generated in the film of PTO2:O-IDTT-IC recombined at a certain level according to the low PLQ efficiency, usually

Table 1. Photovoltaic Parameters of the Devices with PTO2:O-IDTT-4FIC and PTO2:O-IDTT-IC as the Active Layers[a]

condition	V_{OC} [V]	J_{SC} [mA cm^{-2}]	FF [%]	PCE [%]	PCE_{max} [%]
PTO2:O-IDTT-4FIC	0.86 ± 0.03	22.87 ± 1.15	74.11 ± 2.51	14.18 ± 0.33	14.51
PTO2:O-IDTT-IC	1.04 ± 0.02	15.34 ± 0.44	55.43 ± 1.40	8.92 ± 0.19	9.11

[a]The results are averaged from 10 individual devices.

https://dx.doi.org/10.1021/acsami.0c16411
ACS Appl. Mater. Interfaces 2020, 12, 56231−56239

leading to poor device performance.[37] During the exciton dissociation processes, activation energy is required to split excitons to free holes and electrons. To get the activation energy, we performed the $J-V$ measurements with varied substrate temperatures (Figure S6).[38] When the photocurrent is plotted as a function of the inverse substrate temperatures at a certain internal electric field, Arrhenius type behavior is obtained, and the activation energy is determined by fitting the photocurrent with Arrhenius equation presented in Figure 3a,b.[39,40] Two visible features were noticed that (i) the activation energy of the device with O-IDTT-4FIC at a certain internal electric field is lower than that of the device with O-IDTT-IC at the same electric field, and (ii) when the internal electric field is higher, the activation energy is lower. For example, at an internal electric field of 2×10^4 V cm^{-1}, the activation energy of the device with O-IDTT-4FIC is 18.8 meV, which is much lower than the activation energy of the device with O-IDTT-IC (29.8 meV). Moreover, when we plotted the activation energy as a function of the square root of the internal electric field, it is observed that the activation energy follows the Poole–Frenkel-type dependence in the lower electric field regime.

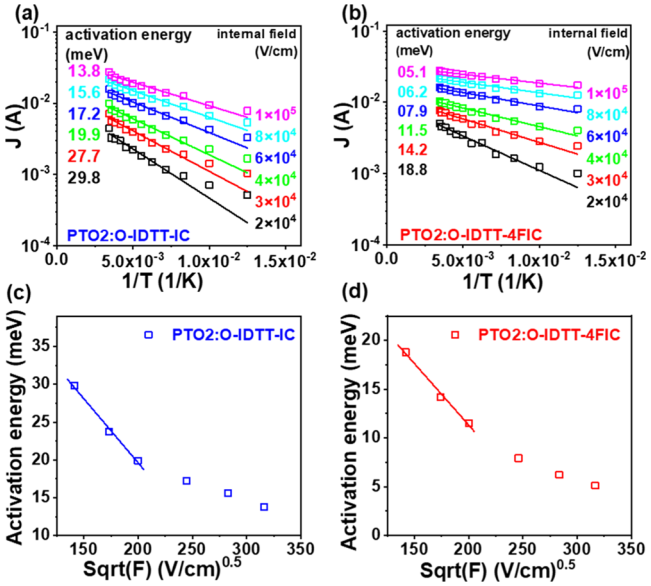

Figure 3. Photocurrent as a function of inverse substrate temperatures at different internal electric fields, (a) devices with PTO2:O-IDTT-4FIC, and (b) devices with PTO2:O-IDTT-ICs. Activation energy as a function of the square root of the internal electric field, (c) devices with PTO2:O-IDTT-4FIC, and (d) devices with PTO2:O-IDTT-IC. The solid lines in (a,b) are fitting to the Arrhenius equation and in (c,d) indicate a Poole–Frenkel type behavior.

By fitting the Pool–Frenkel part, we obtained that the activation energy of the devices with O-IDTT-4FIC and IDTT-IC at zero electric field are 36.7 and 56.5 meV, respectively (Figure 3c,d). Taking into account the exciton recombination and the activation energy needed, the charge carrier generation in the devices with O-IDTT-4FIC is undoubtedly higher than that of the devices with O-IDTT-IC. When the free charge carriers are generated in the active layer, charge recombination plays an important role on whether the charges can be extracted or not. Thus, we next turned to check the recombination patterns in the fluorinated and control devices. By measuring the $J-V$ curves with varied incident light intensities (Figure S7), the fate of free charge carriers in the device is studied. The information of nongeminate recombination can be obtained from the relationships of J_{SC} and V_{OC} as a function of the incident light intensity.

In Figure 4a, J_{SC} of the fluorinated and control devices was plotted as a function of the incident light intensity (I) in a double-logarithm scale. It was reported that the J_{SC} and I follow a power law of $J_{SC} \propto I^{\alpha}$, and thus, the experimental data were fitted. The α value of 1 was fitted for both devices, indicating that the charges are extracted prior to bimolecular recombination in both devices at short-circuit condition.[38] As depicted in Figure 4b, V_{OC} as a function I was plotted in a semi logarithm. The solid lines are the fit to the expression of

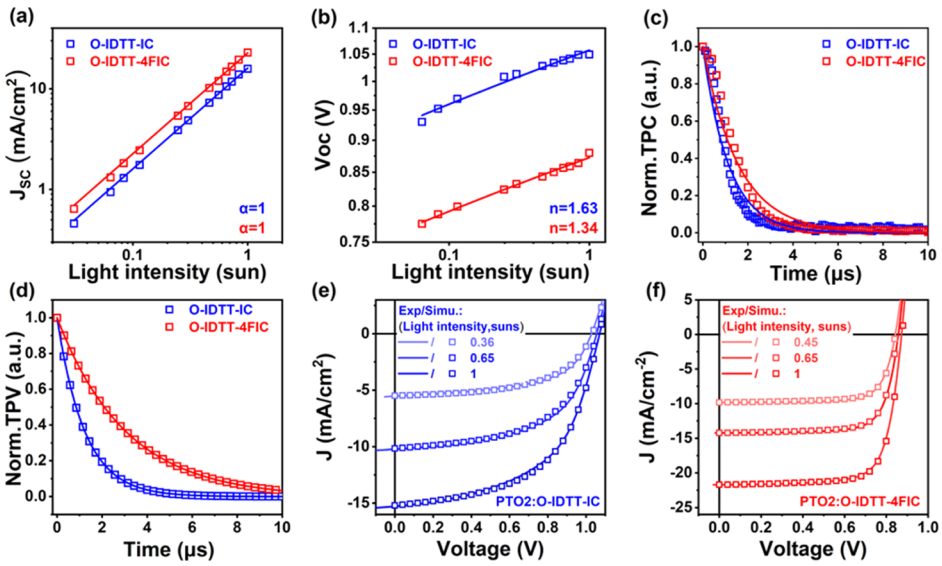

Figure 4. (a) J_{SC} as a function of the incident light intensity for the optimized devices. (b) V_{OC} as a function of the incident light intensity for optimized devices. (c) TPC of the optimized devices. (d) TPV of the optimized devices. 1D drift-diffusion modeling of the $J-V$ curves with (e) PTO2:O-IDTT-IC and (f) PTO2:O-IDTT-IC.

https://dx.doi.org/10.1021/acsami.0c16411
ACS Appl. Mater. Interfaces 2020, 12, 56231–56239

Table 2. Parameters Used in the Drift-Diffusion Simulations of the Devices with O-IDTT-IC and O-IDTT-4FIC[a]

parameter	symbol	PTO2:O-IDTT-IC	PTO2:O-IDTT-4FIC
thickness (nm)	L	130 nm	100 nm
average generationrate (1 sun)	G	7.5×10^{21} cm^{-3} s^{-1}	1.4×10^{22} cm^{-3} s^{-1}
density of states	N_c	9.5×10^{19} cm^{-3}	1.5×10^{20} cm^{-3}
HOMO (effective)	E_{HOMO}	−5.06 eV	−5.06 eV
LUMO (effective)	E_{LUMO}	−3.61 eV	−3.91 eV
relative dielectric constant	ε_r	3.5	3.5
electron mobility*	μ_n	3.82×10^{-5} cm^2 V^{-1} s^{-1}*	5.83×10^{-5} cm^2 V^{-1} s^{-1}*
hole mobility*	μ_p	3.43×10^{-4} cm^2 V^{-1} s^{-1}*	1.62×10^{-4} cm^2 V^{-1} s^{-1}*
bimolecular recombination rate	k_{BR}	9.0×10^{-12} cm^3 s^{-1}	1.5×10^{-12} cm^3 s^{-1}
trap density	N_T	**2.3×10^{12} cm^{-3}**	**2.3×10^{11} cm^{-3}**
trap depth	E_{trap}	0.725	0.575
capture coefficient	$C_n = C_p$	1×10^{-7} cm^3 s^{-1}	1×10^{-7} cm^3 s^{-1}
cathode work function	W_c	−3.61 eV	−3.91 eV
anode work function	W_a	−5.06 eV	−5.06 eV
series resistance	R_{series}	1.35 Ω m^{-2}	1.31 Ω cm^{-2}

[a]The parameters marked with "*" are obtained from experimental.

$V_{OC} \propto n\frac{kT}{q}\ln(I)$, where q, k, and T are the elementary charge, the Boltzmann constant, and the temperature in kelvin, respectively.[41] The n values of 1.34 and 1.63 were fitted for the devices with O-IDTT-4FIC and O-IDTT-IC, implying that both devices suffer a certain extent of trap-assisted recombination at open-circuit condition and the smaller n for the devices with O-IDTT-4FIC indicates the trap-assisted recombination is reduced.

The quantification of the charge extraction and charge carrier lifetime were then evaluated by transient photocurrent (TPC) and transient photovoltage (TPV) measurements.[42] In such measurements, the devices were held at short circuit or open circuit and illuminated by a pulsed laser, and the response signals from the devices to the illuminated light were recorded by an oscilloscope (detail information in Figure S8).[43] The charge extraction time for both systems were derived by fitting the current decay from TPC with monoexponential decay shown in Figure 4c. We found that the charge extraction time is comparable, and the device with O-IDTT-IC is slightly faster. On the other hand, TPV (Figure 4d) provides the information on the number of recombination routes and charge carriers' lifetime. The transient voltage decays were fitted with monoexponential decay and charge carrier lifetimes of 3.04 and 1.22 μs were inferred for the devices with O-IDTT-4FIC and O-IDTT-IC, respectively. The monoexponential fitting tells that only one recombination route dominates the devices, for example, the trap-assisted recombination.[44] Again, the evidently longer charge carrier lifetime for the devices with O-IDTT-4FIC suggests that the trap-assisted recombination was decreased.

Simulations considering charge generation, recombination effects, and the carrier mobilities of the active layer by numerically solving the drift-diffusion equations were performed to get the detailed information about the fluorinated and control devices.[45] To fit the 1D drift-diffusion modeling to the $J-V$ curves with various incident light intensity, we used experimentally measured parameters for the energy levels, refractive index, extinction coefficient, and charge carrier mobility (Figures S3 and S4) and used a fitting procedure to extract the unknown parameters.

The generation of carrier in the active layer was estimated using the measured refractive indexes and transfer matrix modeling.[33] The simulated results are presented in Table 2 and presented in Figure 4e,f. Notably, when the best fitting was obtained, bimolecular recombination is negligible for both the fluorinated and control devices, and trap-assisted recombination is the dominant recombination loss. Specifically, the extracted trap density in the device with O-IDTT-4FIC is 2.3 $\times 10^{11}$ cm^{-3} and in the device with O-IDTT-IC is 2.3 $\times 10^{12}$ cm^{-3}. The simulated results confirm the presence of traps in the devices and are in line with the observations of less trap-assisted recombination based on the V_{OC} *versus* I and the longer charge carrier lifetime fitted from TPV in the device with O-IDTT-4FIC.

Subsequent to the examination of the excitons and charge carriers' behaviors, we turned to find the morphological rationality of all the impacts induced by fluorination. The molecular packing and crystalline properties of pristine and the blend films were investigated by grazing incidence wide-angle X-ray scattering (GIWAXS) technique. Figures 5 and S10

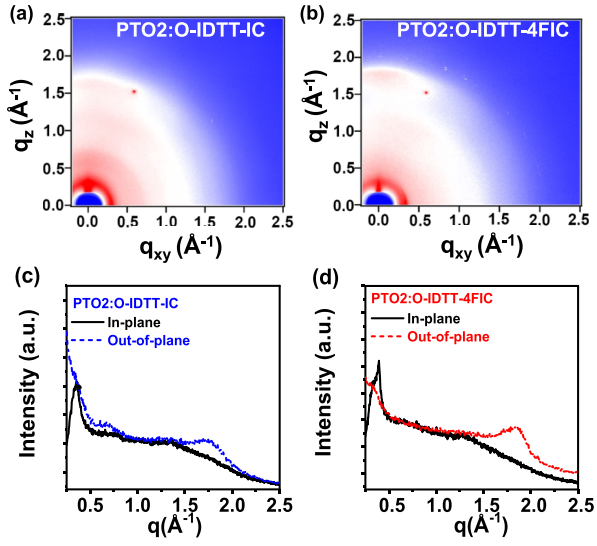

Figure 5. 2D GIWAXS patterns of optimized (a) PTO2:O-IDTT-IC and (b) PTO2:O-IDTT-4FIC blend films. (c,d) IP (black solid lines) and OOP (blue and red dashed lines) profiles for the respective blend films.

https://dx.doi.org/10.1021/acsami.0c16411
ACS Appl. Mater. Interfaces 2020, 12, 56231−56239

show the diffraction patterns and line-cuts in the in-plane (IP) and out-of-plane (OOP) directions. The GIWAX images were recorded with X-rays of 11.57 keV (λ = 1.0716 Å) at 0.13 incidence angle. The pristine PTO2 polymer film showed the first-order (100) diffraction peaks located at $q \sim 0.31$ Å^{-1} (d-spacing ~ 20.03 Å) in IP and $\pi-\pi$ stacking (010) diffraction peak at $q \sim 1.66$ Å^{-1} (d-spacing ~ 3.78 Å) in the OOP direction, indicating a preferential face-on orientation in the PTO2 polymer film. The GIWAXS 2D images of the O-IDTT-4FIC and O-IDTT-IC pristine films clearly illustrated well-developed diffraction patterns with a high order of molecular packing.[46−49] The pristine O-IDTT-IC film has dominated diffraction peaks at $q \sim 0.366$, 0.695, 1.283, 1.381, and 1.172 Å^{-1} in the IP direction. After fluorination, the O-IDTT-4FIC film showed an increase in dominated diffraction peaks at $q \sim$ 0.315, 0.369, 0.523, 0.901, 1.015, 1.251, and 1.286 Å^{-1} in the IP direction. The O-IDTT-4FIC film exhibits a more distinctive diffraction pattern with a higher order of Bragg diffraction peaks compared to the O-IDTT-IC film.

In the blend films, the IP XRD profiles show a stark difference in coherence lengths of (100) diffraction peaks between PTO2:O-IDTT-4FIC and PTO2:O-IDTT-IC. The first order of diffraction peaks, which are composed of 0.33 Å^{-1} from PTO2 and 0.39 Å^{-1} from O-IDTT-4FIC, showed coherence lengths of 9.02 and 9.78 nm, respectively, based on the Scherrer's equation, while the diffraction peaks from PTO2:O-IDTT-IC displayed 6.87 and 4.11 nm from PTO2 and O-IDTT-IC. On the other hand, the OOP XRD profiles of the blend films also exhibit a clear difference of $\pi-\pi$ stacking (010) diffraction peak position. The (010) peak from PTO2:O-IDTT-4FIC is located at 1.84 Å^{-1} that corresponds to the d-spacing of 3.41 Å, but the (010) peak from PTO2:O-IDTT-IC is located at 1.78 Å^{-1} that corresponds to the d-spacing of 3.52 Å. Furthermore, the PTO2:O-IDTT-4FIC film shows a longer crystal coherence length of the (010) diffraction peak (2.32 nm) than that from PTO2:O-IDTT-IC film (1.89 nm). This (010) stacking peak shift indicates that the PTO2:O-IDTT-4FIC blend film contains more compactly packed $\pi-\pi$ stacking planes in OOP with longer coherence length, which is definitely advantageous for charge transport of the vertically stacked photovoltaic devices. These results are in agreement with the electrical properties of the n-type materials that show the more efficient charge transport property of O-IDTT-4FIC than O-IDTT-IC. In addition, more information about the crystallinity of the interface between PTO2 and the receptor, as well as the key parameters other than the crystallinity itself, can be found in the appendix Table S8.

3. CONCLUSIONS

In summary, we investigated the impact of fluorination on the FREAs in high-performed OSCs by systematically comparing the device performances, excitons and charge carriers' behaviors, and the active layer microstructures. The devices with PTO2:O-IDTT-4FIC as the active layer achieved a PCE of 14.5%, outperforming the control devices with PTO2:O-IDTT-IC as the active layer (9.1%). The pronounced photovoltaic performance obtained from the device with O-IDTT-4FIC results from the efficient exciton dissociation efficiency, and less activation energy was required to generate free charge carriers (36.7 meV vs 53.5 meV), much longer charge carrier lifetime (3.04 μs vs 1.22 μs), and significantly reduced trap assisted recombination (trap density 2.3 × 10^{11} cm^{-3} vs 2.3 × 10^{12} cm^{-3}). The superior charge generation and extraction processes originate from the morphological changes that the PTO2:O-IDTT-4FIC blend film contains more compactly packed $\pi-\pi$ stacking planes in OOP with longer coherence length. Our findings provide information about the complex effects of FREA fluorination in high-performance OSCs that can guide the material designs for further performance improvements.

4. EXPERIMENTAL SECTION

4.1. Materials. PTO2 was purchased from Solarmer Co., Ltd. (Beijing, China). PEDOT:PSS and phen-NaDPO were purchased from Energy Chemical., Ltd. DIO and CN additive were supplied by Sigma-Aldrich.

4.2. Device Fabrication and Characterization. The conventional device structure is ITO/PEDOT:PSS/Active Layer/DPO/Ag; the $J-V$ curves of devices were measured under N_2 using a Keithley 2400 source meter. A 300 W xenon arc solar simulator (Enli Technology Co., Ltd) with an AM 1.5 global filter operated at 100 mW cm^{-2} was used to simulate the AM 1.5G solar irradiation. The EQE was performed using certified IPCE equipment (Zolix Instruments, Inc, Solar Cell Scan 100). More details on device fabrication and characterization are given in the Supporting Information.

■ ASSOCIATED CONTENT

Supporting Information

The Supporting Information is available free of charge at https://pubs.acs.org/doi/10.1021/acsami.0c16411.

Experimental details and supplementary characterizations of materials and device performance (PDF)

■ AUTHOR INFORMATION

Corresponding Authors

Ranbir Singh − *Department of Energy and Materials Engineering, Dongguk University, Seoul 04620, Korea*; Email: ranbir@dongguk.edu

Shirong Lu − *Thin-film Solar Technology Research Center, Chongqing Institute of Green and Intelligent Technology, Chinese Academy of Sciences, Chongqing School, University of Chinese Academy of Sciences, Chongqing 400714, China*; orcid.org/0000-0001-6438-1082; Email: lushirong@cigit.ac.cn

Zhipeng Kan − *Thin-film Solar Technology Research Center, Chongqing Institute of Green and Intelligent Technology, Chinese Academy of Sciences, Chongqing School, University of Chinese Academy of Sciences, Chongqing 400714, China*; orcid.org/0000-0003-1378-541X; Email: kanzhipeng@cigit.ac.cn

Authors

Licheng Hou − *Thin-film Solar Technology Research Center, Chongqing Institute of Green and Intelligent Technology, Chinese Academy of Sciences, Chongqing School, University of Chinese Academy of Sciences, Chongqing 400714, China; University of Chinese Academy of Sciences, Beijing 100049, China*

Jie Lv − *Thin-film Solar Technology Research Center, Chongqing Institute of Green and Intelligent Technology, Chinese Academy of Sciences, Chongqing School, University of Chinese Academy of Sciences, Chongqing 400714, China; University of Chinese Academy of Sciences, Beijing 100049, China*

https://dx.doi.org/10.1021/acsami.0c16411
ACS Appl. Mater. Interfaces 2020, 12, 56231−56239

Friso Wobben − *Zernike Institute for Advanced Materials, University of Groningen, Groningen NL-9747AG, The Netherlands*
Vincent M. Le Corre − *Zernike Institute for Advanced Materials, University of Groningen, Groningen NL-9747AG, The Netherlands;* orcid.org/0000-0001-6365-179X
Hua Tang − *Thin-film Solar Technology Research Center, Chongqing Institute of Green and Intelligent Technology, Chinese Academy of Sciences, Chongqing School, University of Chinese Academy of Sciences, Chongqing 400714, China; University of Chinese Academy of Sciences, Beijing 100049, China*
Min Kim − *School of Chemical Engineering, Jeonbuk National University, Jeonju 54896, Republic of Korea*
Fufang Wang − *State Key Laboratory of Precision Spectroscopy, East China Normal University, Shanghai 200062, China*
Haitao Sun − *State Key Laboratory of Precision Spectroscopy, East China Normal University, Shanghai 200062, China;* orcid.org/0000-0003-1471-8876
Wenjing Chen − *Department of Physics, CAS Key Laboratory of Strongly-Coupled Quantum Matter Physics, Hefei National Laboratory for Physical Sciences at the Microscale, University of Science and Technology of China, Hefei, Anhui 230026, China*
Zhengguo Xiao − *Department of Physics, CAS Key Laboratory of Strongly-Coupled Quantum Matter Physics, Hefei National Laboratory for Physical Sciences at the Microscale, University of Science and Technology of China, Hefei, Anhui 230026, China;* orcid.org/0000-0001-6646-1166
Manish Kumar − *Pohang Accelerator Laboratory, Pohang University of Science and Technology, Pohang 37673, Republic of Korea*
Tongle Xu − *Thin-film Solar Technology Research Center, Chongqing Institute of Green and Intelligent Technology, Chinese Academy of Sciences, Chongqing School, University of Chinese Academy of Sciences, Chongqing 400714, China; University of Chinese Academy of Sciences, Beijing 100049, China*
Weimin Zhang − *KAUST Solar Center, King Abdullah University of Science and Technology, Thuwal 23955-6900, Saudi Arabia*
Iain McCulloch − *KAUST Solar Center, King Abdullah University of Science and Technology, Thuwal 23955-6900, Saudi Arabia; Department of Chemistry and Centre for Plastic Electronics, Imperial College London, London SW7 2AZ, U.K.*
Tainan Duan − *Thin-film Solar Technology Research Center, Chongqing Institute of Green and Intelligent Technology, Chinese Academy of Sciences, Chongqing School, University of Chinese Academy of Sciences, Chongqing 400714, China;* orcid.org/0000-0002-6010-4501
Huling Xie − *Thin-film Solar Technology Research Center, Chongqing Institute of Green and Intelligent Technology, Chinese Academy of Sciences, Chongqing School, University of Chinese Academy of Sciences, Chongqing 400714, China*
L. Jan Anton Koster − *Zernike Institute for Advanced Materials, University of Groningen, Groningen NL-9747AG, The Netherlands;* orcid.org/0000-0002-6558-5295

Complete contact information is available at: https://pubs.acs.org/10.1021/acsami.0c16411

Author Contributions

L.H. fabricated and optimized the devices; L.H., J.L. and Z.K. performed the morphology characterization and analysis; H.T. tested the AFM of all materials; F.W. and H.S. did DFT calculation for O-IDTT-4FIC than O-IDTT-IC; W.C. and Z.X. tested PL; T.X. tested the energy level of the material; W.Z., I.M. synthesized the O-IDTT-4FIC and O-IDTT-IC; F.W., V.M.L.C. and L.J.A.K. carried out the 1D drift diffusion simulations; R.S., M.K. and M.K. did the GIWAXS characterization; T.D. and H.X. tested the TEM for all materials; S.L. and Z.K. conceived and directed the project; All authors discussed the results and contributed to the preparation of the manuscript.

Notes

The authors declare no competing financial interest.

■ ACKNOWLEDGMENTS

L.H. and J.L. contributed equally to this work. Z.K. acknowledge the research grants from the National Natural Science Foundation of China (no. 61805245), and CAS Pioneer Hundred Talents Program (Y82A060Q10, Y92A160Q10, E0296102). S.L. thanks the support from the National Youth Thousand Program Project (R52A199Z11), the National Special Funds for Repairing, and Purchasing Scientific Institutions (Y72Z090Q10), and the "Artificial Intelligence" Key Project of Chongqing (no. cstc2017rgzn-zdyfX0030). V.M.L.C. is supported by a grant from STW/NWO (VIDI 13476). The authors thank Huirong Su from Genuine Optronics Ltd. for the measurements of ellipsometry and data analysis.

■ REFERENCES

(1) Tscheuschner, S.; Bässler, H.; Huber, K.; Köhler, A. A Combined Theoretical and Experimental Study of Dissociation of Charge Transfer States at the Donor-Acceptor Interface of Organic Solar Cells. *J. Phys. Chem. B* **2015**, *119*, 10359−10371.
(2) Zhang, H.; Yao, H.; Hou, J.; Zhu, J.; Zhang, J.; Li, W.; Yu, R.; Gao, B.; Zhang, S.; Hou, J. Over 14% Efficiency in Organic Solar Cells Enabled by Chlorinated Nonfullerene Small-Molecule Acceptors. *Adv. Mater.* **2018**, *30*, 1800613.
(3) Feng, K.; Yuan, J.; Bi, Z.; Ma, W.; Xu, X.; Zhang, G.; Peng, Q. Low-Energy-Loss Polymer Solar Cells with 14.52% Efficiency Enabled by Wide-Band-Gap Copolymers. *Iscience* **2019**, *12*, 1.
(4) Li, W.; Ye, L.; Li, S.; Yao, H.; Ade, H.; Hou, J. A High-Efficiency Organic Solar Cell Enabled by the Strong Intramolecular Electron Push-Pull Effect of the Nonfullerene Acceptor. *Adv. Mater.* **2018**, *30*, 1707170.
(5) Luo, Z.; Sun, R.; Zhong, C.; Liu, T.; Zhang, G.; Zou, Y.; Jiao, X.; Min, J.; Yang, C. Altering Alkyl-Chains Branching Positions for Boosting the Performance of Small-molecule Acceptors for Highly Efficient Nonfullerene Organic Solar Cells. *Sci. China: Chem.* **2020**, *63*, 361−369.
(6) Yuan, J.; Zhang, Y.; Zhou, L.; Zhang, G.; Yip, H.-L.; Lau, T.-K.; Lu, X.; Zhu, C.; Peng, H.; Johnson, P. A.; Leclerc, M.; Cao, Y.; Ulanski, J.; Li, Y.; Zou, Y. Single-Junction Organic Solar Cell with over 15% Efficiency Using Fused-Ring Acceptor with Electron-Deficient Core. *Joule* **2019**, *3*, 1140−1151.
(7) Liu, Q.; Jiang, Y.; Jin, K.; Qin, J.; Xu, J.; Li, W.; Xiong, J.; Liu, J.; Xiao, Z.; Sun, K.; Yang, S.; Zhang, X.; Ding, L. 18% Efficiency Organic Solar Cells. *Sci. Bull.* **2020**, *65*, 272−275.
(8) Kim, Y. Y.; Yang, T.-Y.; Suhonen, R.; Valimaki, M.; Maaninen, T.; Kemppainen, A.; Jeon, N. J.; Seo, J. Photovoltaic Devices: Gravure-Printed Flexible Perovskite Solar Cells: Toward Roll-to-Roll Manufacturing. *Adv. Sci.* **2019**, *6*, 1970044.

(9) Kini, G. P.; Jeon, S. J.; Moon, D. K. Design Principles and Synergistic Effects of Chlorination on a Conjugated Backbone for Efficient Organic Photovoltaics: A Critical Review. *Adv. Mater.* **2020**, *32*, 1906175.
(10) Gao, X.; Wu, Y.; Tao, Y.; Huang, W. Conjugated Random Terpolymer Donors towards High-Efficiency Polymer Solar Cells. *Chin. J. Chem.* **2020**, *38*, 601−624.
(11) Wang, Y.; Zhu, Q.; Naveed, H. B.; Zhao, H.; Zhou, K.; Ma, W. Sequential Blade-Coated Acceptor and Donor Enables Simultaneous Enhancement of Efficiency, Stability, and Mechanical Properties for Organic Solar Cells. *Adv. Energy Mater.* **2020**, *10*, 1903609.
(12) Zhu, L.; Zhang, M.; Zhou, G.; Hao, T.; Xu, J.; Wang, J.; Qiu, C.; Prine, N.; Ali, J.; Feng, W.; Gu, X.; Ma, Z.; Tang, Z.; Zhu, H.; Ying, L.; Zhang, Y.; Liu, F. Efficient Organic Solar Cell with 16.88% Efficiency Enabled by Refined Acceptor Crystallization and Morphology with Improved Charge Transfer and Transport Properties. *Adv. Energy Mater.* **2020**, *10*, 1904234.
(13) Cai, G.; Wang, W.; Zhou, J.; Xiao, Y.; Liu, K.; Xie, Z.; Lu, X.; Lian, J.; Zeng, P.; Wang, Y.; Zhan, X. Comparison of Linear- and Star-Shaped Fused-Ring Electron Acceptors. *ACS Mater. Lett.* **2019**, *1*, 367.
(14) Albrecht, S.; Janietz, S.; Schindler, W.; Frisch, J.; Kurpiers, J.; Kniepert, J.; Inal, S.; Pingel, P.; Fostiropoulos, K.; Koch, N.; Neher, D. Fluorinated Copolymer PCPDTBT with Enhanced Open-Circuit Voltage and Reduced Recombination for Highly Efficient Polymer Solar Cells. *J. Am. Chem. Soc.* **2012**, *134*, 14932−14944.
(15) Kawashima, K.; Fukuhara, T.; Suda, Y.; Suzuki, Y.; Koganezawa, T.; Yoshida, H.; Ohkita, H.; Osaka, I.; Takimiya, K. Implication of Fluorine Atom on Electronic Properties, Ordering Structures, and Photovoltaic Performance in Naphthobisthiadiazole-Based Semiconducting Polymers. *J. Am. Chem. Soc.* **2016**, *138*, 10265−10275.
(16) Wolf, J.; Cruciani, F.; El Labban, A.; Beaujuge, P. M. Wide Band-Gap 3,4-Difluorothiophene-Based Polymer with 7% Solar Cell Efficiency: An Alternative to P3HT. *Chem. Mater.* **2015**, *27*, 4184−4187.
(17) Bauer, N.; Zhang, Q.; Rech, J. J.; Dai, S.; Peng, Z.; Ade, H.; Wang, J.; Zhan, X.; You, W. The Impact of Fluorination on Both Donor Polymer and Non-Fullerene Acceptor: The More Fluorine, the Merrier. *Nano Res.* **2019**, *12*, 2400−2405.
(18) Stuart, A. C.; Tumbleston, J. R.; Zhou, H.; Li, W.; Liu, S.; Ade, H.; You, W. Fluorine Substituents Reduce Charge Recombination and Drive Structure and Morphology Development in Polymer Solar Cells. *J. Am. Chem. Soc.* **2013**, *135*, 1806−1815.
(19) Han, X.; Zhu, J.; Xiao, Y.; Jiang, H.; Zhang, Z.; Wang, J.; Li, Z.; Lin, Y.; Lu, X.; Zhan, X. An Alkoxy-Solubilizing Decacyclic Electron Acceptor for Efficient Ecofriendly As-Cast Blade-Coated Organic Solar Cells. *Sol. RRL* **2020**, *4*, 2000108.
(20) Bin, H.; Zhang, Z.-G.; Gao, L.; Chen, S.; Zhong, L.; Xue, L.; Yang, C.; Li, Y. Non-Fullerene Polymer Solar Cells Based on Alkylthio and Fluorine Substituted 2D-Conjugated Polymers Reach 9.5% Efficiency. *J. Am. Chem. Soc.* **2016**, *138*, 4657−4664.
(21) Dai, S.; Zhao, F.; Zhang, Q.; Lau, T.-K.; Li, T.; Liu, K.; Ling, Q.; Wang, C.; Lu, X.; You, W.; Zhan, X. Fused Nonacyclic Electron Acceptors for Efficient Polymer Solar Cells. *J. Am. Chem. Soc.* **2017**, *139*, 1336−1343.
(22) Li, W.; Albrecht, S.; Yang, L.; Roland, S.; Tumbleston, J. R.; McAfee, T.; Yan, L.; Kelly, M. A.; Ade, H.; Neher, D.; You, W. Mobility-Controlled Performance of Thick Solar Cells Based on Fluorinated Copolymers. *J. Am. Chem. Soc.* **2014**, *136*, 15566−15576.
(23) Dai, S.; Zhou, J.; Chandrabose, S.; Shi, Y.; Han, G.; Chen, K.; Xin, J.; Liu, K.; Chen, Z.; Xie, Z.; Ma, W.; Yi, Y.; Jiang, L.; Hodgkiss, J. M.; Zhan, X. High-Performance Fluorinated Fused-Ring Electron Acceptor with 3D Stacking and Exciton/Charge Transport. *Adv. Mater.* **2020**, *32*, 2000645.
(24) Duan, T.; Gao, J.; Babics, M.; Kan, Z.; Zhong, C.; Singh, R.; Yu, D.; Lee, J.; Xiao, Z.; Lu, S. Difluorinated Oligothiophenes for High-Efficiency All-Small-Molecule Organic Solar Cells: Positional Isomeric Effect of Fluorine Substitution on Performance Variations. *Sol. RRL* **2020**, *4*, 1900472.
(25) Tang, H.; Yan, C.; Karuthedath, S.; Yin, H.; Gao, Y.; Gao, J.; Zhang, L.; Huang, J.; So, S. K.; Kan, Z.; Laquai, F.; Li, G.; Lu, S. Deciphering the Role of Fluorination: Morphological Manipulation Prompts Charge Separation and Reduces Carrier Recombination in All-Small-Molecule Photovoltaics. *Sol. RRL* **2020**, *4*, 1900528.
(26) Fan, Q.; Su, W.; Zhang, M.; Wu, J.; Jiang, Y.; Guo, X.; Liu, F.; Russell, T. P.; Zhang, M.; Li, Y. Synergistic Effects of Side-Chain Engineering and Fluorination on Small Molecule Acceptors to Simultaneously Broaden Spectral Response and Minimize Voltage Loss for 13.8% Efficiency Organic Solar Cells. *Sol. RRL* **2019**, *3*, 1900169.
(27) Wan, S.-S.; Xu, X.; Jiang, Z.; Yuan, J.; Mahmood, A.; Yuan, G.-Z.; Liu, K.-K.; Ma, W.; Peng, Q.; Wang, J.-L. A Bromine and Chlorine Concurrently Functionalized end Group for Benzo[1,2-b:4,5-b′]-Diselenophene-Based Non-fluorinated Acceptors: A New Hybrid Strategy to Balance the Crystallinity and Miscibility of Blend Films for Enabling Highly Efficient Polymer Solar Cells. *J. Mater. Chem. A* **2020**, *8*, 4856−4867.
(28) Zhao, W.; Li, S.; Yao, H.; Zhang, S.; Zhang, Y.; Yang, B.; Hou, J. Molecular Optimization Enables over 13% Efficiency in Organic Solar Cells. *J. Am. Chem. Soc.* **2017**, *139*, 7148−7151.
(29) Gao, H.-H.; Sun, Y.; Wan, X.; Ke, X.; Feng, H.; Kan, B.; Wang, Y.; Zhang, Y.; Li, C.; Chen, Y. A New Nonfullerene Acceptor with Near Infrared Absorption for High Performance Ternary-Blend Organic Solar Cells with Efficiency over 13. *Adv. Sci.* **2018**, *5*, 1800307.
(30) Becke, A. D. Density-Functional Thermochemistry. III. The Role of Exact Exchange. *J. Chem. Phys.* **1993**, *98*, 5648−5652.
(31) Lee, C.; Yang, W.; Parr, R. G. Development of the Colle-Salvetti Correlation-Energy Formula into a Functional of the Electron Density. *Phys. Rev. B: Condens. Matter Mater. Phys.* **1988**, *37*, 785−789.
(32) Grimme, S.; Ehrlich, S.; Goerigk, L. Effect of the Damping Function in Dispersion Corrected Density Functional Theory. *J. Comput. Chem.* **2011**, *32*, 1456−1465.
(33) Burkhard, G. F.; Hoke, E. T.; McGehee, M. D. Accounting for Interference, Scattering, and Electrode Absorption to Make Accurate Internal Quantum Efficiency Measurements in Organic and Other Thin Solar Cells. *Adv. Mater.* **2010**, *22*, 3293−3297.
(34) Firdaus, Y.; Maffei, L. P.; Cruciani, F.; Müller, M. A.; Liu, S.; Lopatin, S.; Wehbe, N.; Ndjawa, G. O. N.; Amassian, A.; Laquai, F.; Beaujuge, P. M. Polymer Main-Chain Substitution Effects on the Efficiency of Nonfullerene BHJ Solar Cells. *Adv. Energy Mater.* **2017**, *7*, 1700834.
(35) Karki, A.; Vollbrecht, J.; Gillett, A. J.; Selter, P.; Lee, J.; Peng, Z.; Schopp, N.; Dixon, A. L.; Schrock, M.; Nádaždy, V.; Schauer, F.; Ade, H.; Chmelka, B. F.; Bazan, G. C.; Friend, R. H.; Nguyen, T.-Q. Unifying Charge Generation, Recombination, and Extraction in Low-Offset Non-Fullerene Acceptor Organic Solar Cells. *Adv. Energy Mater.* **2020**, *10*, 2001203.
(36) Karuthedath, S.; Gorenflot, J.; Firdaus, Y.; Chaturvedi, N.; De Castro, C. S. P.; Harrison, G. T.; Khan, J. I.; Markina, A.; Balawi, A. H.; Peña, T. A. D.; Liu, W.; Liang, R.-Z.; Sharma, A.; Paleti, S. H. K.; Zhang, W.; Lin, Y.; Alarousu, E.; Anjum, D. H.; Beaujuge, P. M.; De Wolf, S.; McCulloch, I.; Anthopoulos, T. D.; Baran, D.; Andrienko, D.; Laquai, F. Intrinsic Efficiency Limits in Low-bandgap Non-fullerene Acceptor Organic Solar Cells. *Nat. Mater.* **2020**, DOI: 10.1038/s41563-020-00835-x.
(37) Alqahtani, O.; Babics, M.; Gorenflot, J.; Savikhin, V.; Ferron, T.; Balawi, A. H.; Paulke, A.; Kan, Z.; Pope, M.; Clulow, A. J.; Wolf, J.; Burn, P. L.; Gentle, I. R.; Neher, D.; Toney, M. F.; Laquai, F.; Beaujuge, P. M.; Collins, B. A. Mixed Domains Enhance Charge Generation and Extraction in Bulk-Heterojunction Solar Cells with Small-Molecule Donors. *Adv. Energy Mater.* **2018**, *8*, 1702941.
(38) Li, J.; Liang, Z.; Li, X.; Li, H.; Wang, Y.; Qin, J.; Tong, J.; Yan, L.; Bao, X.; Xia, Y. Insights into Excitonic Dynamics of Terpolymer-Based High-Efficiency Nonfullerene Polymer Solar Cells: Enhancing

the Yield of Charge Separation States. *ACS Appl. Mater. Interfaces* **2020**, *12*, 8475−8484.
(39) Athanasopoulos, S.; Schauer, F.; Nádaždy, V.; Weiß, M.; Kahle, F. J.; Scherf, U.; Bässler, H.; Köhler, A. What is the Binding Energy of a Charge Transfer State in an Organic Solar Cell? *Adv. Energy Mater.* **2019**, *9*, 1900814.
(40) Lv, J.; Feng, Y.; Fu, J.; Gao, J.; Singh, R.; Kumar, M.; Kim, M.; Tang, H.; Lu, S.; Zhang, W.; McCulloch, I.; Li, J.; Kan, Z. Energetic Disorder and Activation Energy in Efficient Ternary Organic Solar Cells with Nonfullerene Acceptor Eh-IDTBR as the Third Component. *Sol. RRL* **2019**, *4*, 1900403.
(41) Gong, Y.; Kan, Z.; Xu, W.; Wang, Y.; AlShammari, S. H.; Laquai, F.; Lai, W.-Y.; Huang, W. Wide-Bandgap Small Molecular Acceptors Based on a Weak Electron-Withdrawing Moiety for Efficient Polymer Solar Cells. *Sol. RRL* **2018**, *2*, 1800120.
(42) Yang, Y.; Chen, W.; Dou, L.; Chang, W.-H.; Duan, H.-S.; Bob, B.; Li, G.; Yang, Y. High-Performance Multiple-Donor Bulk Heterojunction Solar Cells. *Nat. Photonics* **2015**, *9*, 190−198.
(43) Liang, R.-Z.; Babics, M.; Seitkhan, A.; Wang, K.; Geraghty, P. B.; Lopatin, S.; Cruciani, F.; Firdaus, Y.; Caporuscio, M.; Jones, D. J.; Beaujuge, P. M. Additive-Morphology Interplay and Loss Channels in "All-Small-Molecule" Bulk-heterojunction (BHJ) Solar Cells with the Nonfullerene Acceptor IDTTBM. *Adv. Funct. Mater.* **2017**, *28*, 1705464.
(44) Li, Z.; Gao, F.; Greenham, N. C.; McNeill, C. R. Comparison of the Operation of Polymer/Fullerene, Polymer/Polymer, and Polymer/Nanocrystal Solar Cells: A Transient Photocurrent and Photovoltage Study. *Adv. Funct. Mater.* **2011**, *21*, 1419−1431.
(45) Koster, L. J. A.; Smits, E. C. P.; Mihailetchi, V. D.; Blom, P. W. M. Device Model for the Operation of Polymer/Fullerene Bulk Heterojunction Solar Cells. *Phys. Rev. B: Condens. Matter Mater. Phys.* **2005**, *72*, 085205.
(46) A 1D Drift-Diffusion Simulator for Semiconductor Devices (LEDs, Solar Cells, Diodes, Organics, Perovskites). https://github.com/kostergroup/SIMsalabim.
(47) Richter, L. J.; DeLongchamp, D. M.; Amassian, A. Morphology Development in Solution-Processed Functional Organic Blend Films: An In Situ Viewpoint. *Chem. Rev.* **2017**, *117*, 6332−6366.
(48) Li, J.; Wang, Y.; Liang, Z.; Qin, J.; Ren, M.; Tong, J.; Yang, C.; Yang, C.; Bao, X.; Xia, Y. Non-Toxic Green Food Additive Enables Efficient Polymer Solar Cells Through Adjusting the Phase Composition Distribution and Boosting Charge Transport. *J. Mater. Chem. C* **2020**, *8*, 2483−2490.
(49) Tang, H.; Chen, H.; Yan, C.; Huang, J.; Fong, P.; Lv, J.; Hu, D.; Singh, R.; Kumar, M.; Xiao, Z.; Kan, Z.; Lu, S.; Li, G. Delicate Morphology Control Triggers 14.7% Efficiency All-Small-Molecule Organic Solar Cells. *Adv. Energy Mater.* **2020**, *10*, 2001076.

https://dx.doi.org/10.1021/acsami.0c16411
ACS Appl. Mater. Interfaces 2020, 12, 56231−56239